Target Tracking in State Dependent Wake Clutter

Edmund Brekke
University Graduate Center
Kjeller, Norway
Email: edmund@unik.no

Oddvar Hallingstad
University Graduate Center
Kjeller, Norway
Email: oh@unik.no

John Glattetre
Kongsberg Maritime
Horten, Norway
Email: jhg@kongsberg.com

***Abstract*— Tracking methods attempt to follow the movement of a target of interest while suppressing irrelevant clutter. A particularly troublesome source of clutter is wakes that appear behind the target. This problem arises in sonar tracking of human divers, in the tracking of boats using surveillance radars, and also in radar tracking of ballistic missiles. Previous research has integrated a solution to this problem in the popular Probabilistic Data Association filter (PDAF).**

This paper proposes a new solution to this problem in the same framework. While previous research has used an approach described as probabilistic editing, the new solution solves the wake problem in a Bayesian framework by means of marginalization.

Monte-Carlo simulations show that the new solution provides significantly increased robustness as compared to both the standard PDAF and the probabilistic editing approach. As the new solution has improved theoretical underpinnings, we hope that it can be useful for further research on tracking in the presence of wake clutter.

I. INTRODUCTION

In harbor surveillance, sensors such as radars and sonars are used to detect and track various targets. Conventional tracking methods work on point measurements extracted from the radar or sonar images. The tracking method attempts to associate these correctly to targets of interest and to clutter, which by definition is not of interest.

Clutter is caused by several sources. There will always be some background noise that is not filtered out by the detection operation, as no detector can achieve unity detection probability for a non-unity false alarm rate [1]. Acoustic reverberation or radar backscatter from the sea surface may cause more troublesome clutter, which often is characterized by heavy-tailed amplitude distributions [2].

Almost all literature on target tracking has so far assumed that the clutter is independent of the target. An important counter-example to this assumption is targets with wakes. Such targets can be scuba divers in sonar data, and ships or missiles in radar data. The wake of a target can be a much more powerful source of clutter than background noise or arbitrary backscatter.

The background for our work on wake targets can be traced back to [3], in which it was suggested to treat wake measurements as clutter, thereby enabling the tracking algorithm to filter out such measurements using probabilistic editing. In [4] this approach was integrated into an operational data association algorithm, namely the classical Probabilistic Data Association filter (PDAF) [5]. Further extensions of this work treated multiple targets [6] and multiple sensors [7].

The intuition behind any solution to the wake problem is that measurements behind the predicted target position are more likely to originate from the wake than measurements in front of the predicted target position. Intuition also tells us that the further behind a measurement is, the more likely it is to be from the wake. In [3] and [4] this intuitive notion was quantified by assigning wake measurements a spatial probability density function (pdf) in the shape of a linear ramp.

An objection to that approach is that the intensity of the wake cannot be expected to increase indefinitely as one moves backwards from the target. Rather, physical considerations leads to a decaying wake model, or possibly an approximately flat wake model if the decay is slow. Another objection to the approach of [3] and [4] is their usage of probabilistic editing. The linear ramp does not have any further justification than the ad-hoc reasoning in the previous paragraph, and one may ask whether a more rigorous approach can be developed.

In this paper a different solution to the wake problem is developed. This solution can be summarized by two key ideas. First, the *wake pdf* is assumed flat. Second, the wake is assumed to begin at the true but unknown *target position*, and not at the *target prediction* as implicitly assumed in [4]. A backwards increasing *clutter pdf* is then obtained by marginalization over the predicted pdf of the target.

Tracking methods can be classified into parametric and non-parametric tracking methods. Parametric tracking methods assume knowledge about the clutter cardinality distribution or point mass function (pmf). Non-parametric tracking methods do not assume any knowledge about it, and assign the clutter cardinality a non-informative or diffuse pmf. Using a flat wake model allows us to specify the wake as a region with a well-defined clutter intensity λ_w which is higher than the surrounding clutter intensity λ_0. The flat wake model can therefore be integrated into parametric tracking methods. This is important since most tracking methods are parametric. On the other hand, it is also important to validate that the proposed approach is useful for non-parametric tracking methods. Therefore we develop the new solution to the wake problem in the framework of the non-parametric PDAF, which also was used in [4].

The work presented here addresses some of the same problems as the references [8 pp. 424-426] or [9], in which a random set approach to extraneous target measurements were developed. This leads to a more general and abstract methodology of which wake clutter can be considered a special case. However, our aim is not to elaborate such a special case, but rather to improve the treatment of wake clutter in the conventional framework of the PDAF.

This paper investigates three versions of the PDAF: The classical non-parametric PDAF, the modified PDAF of [4] which here is termed WPDAF-1, and the tracker developed in this paper, which we call WPDAF-2. The paper is organized as follows: Section II presents background material, including the PDAF tracking method and how it has been modified in previous research on tracking of wake targets. In Section III an alternative modification of the PDAF is developed. In Section IV the tracking methods are tested on simulated data. A brief conclusion is found in Section V. Details regarding the derivations of the PDAF and the wake model are left for the Appendix.

II. Background

This section presents the conventional PDAF method and a modified version of this method that was used to track wake targets in [4].

A. Kinematics and measurement model

We assume that there is one and only one target in the surveillance region, whose kinematic state is denoted by the vector $\boldsymbol{x}_k$. The state contains position $\boldsymbol{\rho}_k$ and possibly other variables such as velocity, acceleration, heading and so on, so that $\boldsymbol{x}_k = [\boldsymbol{\rho}_k^T, \ldots]^T$. For ease of presentation the kinematic transition prior is assumed linear,

$$\boldsymbol{x}_k = \boldsymbol{F}\boldsymbol{x}_{k-1} + \boldsymbol{v}_k, \;\; \boldsymbol{v}_k \sim \mathcal{N}(\boldsymbol{0}, \boldsymbol{Q}). \tag{1}$$

Measurement vectors $\boldsymbol{z}_k$ of the target are also related linearly to the target state:

$$\boldsymbol{z}_k = \boldsymbol{H}\boldsymbol{x}_k + \boldsymbol{w}_k = \boldsymbol{\rho}_k + \boldsymbol{w}_k, \;\; \boldsymbol{w}_k \sim \mathcal{N}(\boldsymbol{0}, \boldsymbol{R}). \tag{2}$$

Notice that the matrix $\boldsymbol{H}$ is supposed to be constructed in such a way that the measurement vector contains only the position of the target corrupted by the measurement noise $\boldsymbol{w}_k$. We believe that extensions of our work to measurements including Doppler, amplitude and so on are quite straightforward, but for simplicity such cases are not to be considered here. Also notice that measurements in polar coordinates can easily be converted to measurements obeying (2) as explained in [5 pp. 38-41].

For uncorrelated $\boldsymbol{v}_k$ and $\boldsymbol{w}_k$ the filtering problem posed by (1) and (2) is optimally solved by the Kalman filter [10]. In reality one does not have a single measurement at each time, but a set of validated measurements $\boldsymbol{Z}_k = \{\boldsymbol{z}_k(1), \ldots, \boldsymbol{z}_k(m_k)\}$ which may or may not include a true measurement from the target. The rest of the measurements are considered "clutter", and data association is needed to discriminate against such false measurements.

B. Probabilistic data association

The PDAF is one of today's most popular tracking algorithms due to its pragmatic compromise between efficiency and robustness. It is a suboptimal algorithm which at each time step collapses the target state posterior pdf into a single Gaussian which then is propagated to the next time step. Thus the past information about the target at time step k is summarized by

$$p(\boldsymbol{x}_k|\boldsymbol{Z}^{k-1}) \approx \mathcal{N}(\boldsymbol{x}_k\,;\,\hat{\boldsymbol{x}}_{k|k-1}, \boldsymbol{P}_{k|k-1}), \tag{3}$$

where $\boldsymbol{Z}^{k-1} = (\boldsymbol{Z}_1, \ldots, \boldsymbol{Z}^{k-1})$ is the collection of all previous measurements. The lumping implied by (3) is done by expressing the state estimate at time k as a weighted average of the prediction $\hat{\boldsymbol{x}}_{k|k-1}$ and state estimates conditioned on the latest measurements $\boldsymbol{z}_k(i)$. This leads to the following Kalman filter-like equations for prediction and measurement update of the state estimate $\hat{\boldsymbol{x}}_{k|k}$ and its associated covariance $\boldsymbol{P}_{k|k}$:

$$\begin{aligned}
\hat{\boldsymbol{x}}_{k|k-1} &= \boldsymbol{F}\hat{\boldsymbol{x}}_{k-1|k-1} \\
\boldsymbol{P}_{k|k-1} &= \boldsymbol{F}\boldsymbol{P}_{k-1|k-1}\boldsymbol{F}^T + \boldsymbol{Q} \\
\hat{\boldsymbol{x}}_{k|k} &= \hat{\boldsymbol{x}}_{k|k-1} + \boldsymbol{K}_k \sum_{i=1}^{m_k} \beta_k(i)\boldsymbol{\nu}_k(i) \\
\boldsymbol{P}_{k|k} &= \boldsymbol{P}_{k|k-1} - (1-\beta_k(0))\boldsymbol{K}_k\boldsymbol{S}_k\boldsymbol{K}_k^T + \tilde{\boldsymbol{P}}_k
\end{aligned} \tag{4}$$

where

$$\begin{aligned}
\boldsymbol{K}_k &= \boldsymbol{P}_{k|k-1}\boldsymbol{H}^T\boldsymbol{S}_k^{-1} \\
\boldsymbol{S}_k &= \boldsymbol{H}\boldsymbol{P}_{k|k-1}\boldsymbol{H}^T + \boldsymbol{R}_k \\
\boldsymbol{\nu}_k(i) &= \boldsymbol{z}_k(i) - \boldsymbol{H}\hat{\boldsymbol{x}}_{k|k-1} = \boldsymbol{z}_k(i) - \hat{\boldsymbol{z}}_{k|k-1} \\
\tilde{\boldsymbol{P}}_k &= \boldsymbol{K}_k \left[\sum_{i=1}^{m_k} \beta_k(i)\boldsymbol{\nu}_k(i)\boldsymbol{\nu}_k(i)^T - \boldsymbol{\nu}_k\boldsymbol{\nu}_k^T\right]\boldsymbol{K}_k^T \\
\boldsymbol{\nu}_k &= \sum_{i=1}^{m_k} \beta_k(i)\boldsymbol{\nu}_k(i).
\end{aligned} \tag{5}$$

The index i ranges over all m_k extracted and validated measurements inside a validation gate $\mathcal{G}$, defined by

$$\mathcal{G} \,:\, (\boldsymbol{z}_k - \boldsymbol{H}\hat{\boldsymbol{x}}_{k|k-1})^T\boldsymbol{\Psi}_k^{-1}(\boldsymbol{z}_k - \boldsymbol{H}\hat{\boldsymbol{x}}_{k|k-1}) < 1 \tag{6}$$

where $\boldsymbol{\Psi}_k = g^2\boldsymbol{S}_k$ and the scalar g is called the gate size.

The association probabilities $\beta_k(i) \triangleq P\{\theta_k(i)|\boldsymbol{Z}^k\}$ in (4) are the probabilities of the following mutually exclusive and exhaustive events

$\theta_k(0)$	No measurement originates from the target
$\theta_k(1)$	Measurement 1 originates from the target
$\vdots$	
$\theta_k(m_k)$	Measurement m_k originates from the target.

The PDAF comes in a parametric and in a non-parametric version. The parametric version assumes that the number of clutter measurements is Poisson distributed (c.f. Section III-C). However, since it can be very difficult to estimate the parameters of this Poisson process, a non-parametric version is commonly used instead. The non-parametric PDAF treats the clutter intensity as unknown by assigning it a flat pmf:

$$\mu(0) = \mu(1) = \ldots = \mu(m-1) = \mu(m) = \mu(m+1) = \ldots.$$

For the non-parametric PDAF, as derived under standard assumptions (c.f. Appendix A), the association probabilities can be written

$$\beta_k(0) = \frac{\delta}{\delta + \sum_{j=1}^{m_k} l(j)} \tag{7}$$

$$\beta_k(i) = \frac{l(i)}{\delta + \sum_{j=1}^{m_k} l(j)} \tag{8}$$

where

$$\delta = m_k \frac{1 - P_{\mathrm{D}} P_{\mathrm{G}}}{P_{\mathrm{D}} P_{\mathrm{G}}}. \tag{9}$$

The constant P_{D} is the probability of detection while P_{G} is the probability that a true detected measurement is inside the gate. P_{D} is a tuning parameter assumed known, while P_{G} can be calculated from g as explained in [5 p. 96]. The likelihood ratio $l(i)$ is defined as

$$l(i) = \frac{p(\boldsymbol{z}_k(i) | \boldsymbol{z}_k(i) \text{ is from target})}{p(\boldsymbol{z}_k(i) | \boldsymbol{z}_k(i) \text{ is from clutter})}. \tag{10}$$

For the conventional PDAF we have

$$l(i) = \frac{p_1(i)}{p_0(i)} \tag{11}$$

where

$$p_1(i) = \frac{1}{P_{\mathrm{G}}} \mathcal{N}(\boldsymbol{z}_k(i)\,;\, \hat{\boldsymbol{z}}_{k|k-1}, \boldsymbol{S}_k) \tag{12}$$

and

$$p_0(i) = \frac{1}{V} = \frac{1}{\pi g^2 |\boldsymbol{S}_k|^{1/2}} \tag{13}$$

when the dimension of $\boldsymbol{z}_k(i)$ is 2. In Sections II-C and III-C alternatives to the uniform clutter pdf of (13) are suggested.

C. Mitigation of a wake by means of probabilistic editing

In [4] it was noticed that the PDAF had trouble tracking a human scuba diver due to a trailing "wake" of air bubbles. The proposed solution was to replace the uniform clutter pdf $p_0(i) = 1/V_k$ with a mixture

$$p_m(i) \triangleq (1 - P_{\mathrm{B}}) \frac{1}{V_k} + \frac{P_{\mathrm{B}}}{P_{\mathrm{GB}}} p_b(\boldsymbol{z}_k(i)). \tag{14}$$

It consists of the conventional flat clutter pdf and a linear ramp $p_b(\cdot)$ which increases backwards behind the predicted target position. P_{B} is a mixture constant related to the wake intensity while P_{GB} is a normalization constant. The ramp is before normalization given by

$$p_b(\boldsymbol{z}) = \begin{cases} z^{\tilde{y}}/(AB^2) & \text{if } 0 < z^{\tilde{y}} < B \text{ and } \|z^{\tilde{x}}\| < A \\ 0 & \text{otherwise} \end{cases}$$

where the wake-oriented coordinates $z^{\tilde{x}}$ and $z^{\tilde{y}}$ are yet to be properly introduced in Section III-A. It is shown in [11] that the normalization constant P_{GB} can be written

$$\begin{aligned} P_{\mathrm{GB}} &= \int_{\mathcal{G}} p_b(\boldsymbol{z}) \mathrm{d}\boldsymbol{z} \\ &= \frac{2}{3AB^2} \det(\boldsymbol{\Lambda}) \left\| \boldsymbol{\Lambda}^{-\frac{1}{2}} \boldsymbol{M}^{\mathsf{T}} \boldsymbol{R}\left(\frac{\pi}{2}\right) \boldsymbol{u} \right\| \end{aligned} \tag{15}$$

where $(\boldsymbol{\Lambda}, \boldsymbol{M})$ is the diagonalization of $\boldsymbol{\Psi}$ as in (33). To summarize, the tracking method of [4] results when the likelihood ratio in (7) and (8) is chosen to be

$$l(i) = \frac{p_1(i)}{p_m(i)}. \tag{16}$$

We refer to this tracking method as WPDAF-1.

III. Mitigation of a wake by means of marginalization

The mixture (14) is a valid pdf, but it is not the spatial pdf of clutter measurements under any reasonable model of the wake. Previous papers on wake targets [3,6,4,7] have not made any attempts at providing a probabilistic model for the wake. The rationale behind this section is that a more robust tracking method may be obtained if the ramp in (14) is replaced by a pdf which actually models the wake.

A. Geometry of the wake model

As the simplest yet plausible model imaginable we suggest a flat wake model. Wake measurements are uniformly distributed in a rectangular region behind the target with width $2A$ and length B. The notion of "behind" is given by the heading unit vector $\boldsymbol{u}_k$, which points in the opposite direction of the wake. We assume this vector known. This can to some degree be justified by the fact that for a slowly manoeuvering target several scans can be used to obtain a good estimate of this vector. This was actually done in [4] as well. It is useful to employ a wake oriented coordinate system $(\tilde{x}, \tilde{y})$ with unit vectors

$$\boldsymbol{e}_k^{\tilde{x}} = \boldsymbol{R}(\pi/2)\boldsymbol{u}_k \;\;,\;\; \boldsymbol{e}_k^{\tilde{y}} = -\boldsymbol{u}_k \tag{17}$$

in addition to the fixed (x, y)-system. Here $\boldsymbol{R}(\alpha)$ denotes a two-dimensional rotation matrix corresponding to α radians. When a point $\boldsymbol{\rho}_k$ is decomposed in the $(\tilde{x}, \tilde{y})$-system we will denote its components by $\rho_k^{\tilde{x}}$ and $\rho_k^{\tilde{y}}$:

$$\begin{aligned} \rho_k^{\tilde{x}} &= (\boldsymbol{z} - \boldsymbol{H}\hat{\boldsymbol{x}}_{k|k-1})^{\mathsf{T}} \boldsymbol{R}(\pi/2)\, \boldsymbol{u}_k \\ \rho_k^{\tilde{y}} &= -\,(\boldsymbol{z} - \boldsymbol{H}\hat{\boldsymbol{x}}_{k|k-1})^{\mathsf{T}} \boldsymbol{u}_k. \end{aligned} \tag{18}$$

The entire wake region is denoted $\mathcal{W}$, and it splits the validation gate into a back region $\mathcal{C}$ and a front region $\mathcal{D}$,

$$\mathcal{C} = \mathcal{G} \cap \mathcal{W}, \;\; \mathcal{D} = \mathcal{G} \setminus \mathcal{C}, \tag{19}$$

where "\" is the set difference operator. Notice that since $\mathcal{W}$ depends on the state $\boldsymbol{x}_k$, the regions $\mathcal{C}$ and $\mathcal{D}$ depend on $\boldsymbol{x}_k$ as well. The regions do of course also depend on $\hat{\boldsymbol{x}}_{k|k-1}$, but this dependency poses less of a challenge since $\hat{\boldsymbol{x}}_{k|k-1}$ is given and not random when conditioned on $\boldsymbol{Z}^{k-1}$. See Figure 1 for an illustration of the geometry.

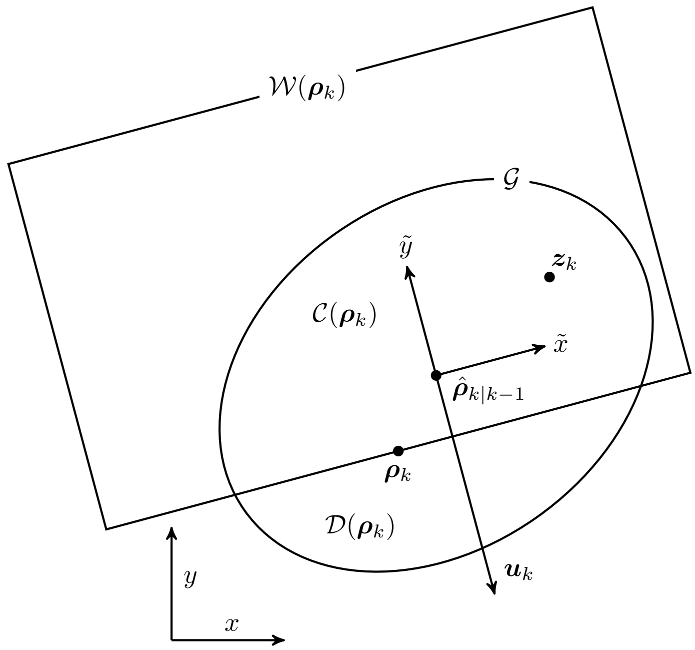

Fig. 1. Illustration of the validation gate $\mathcal{G}$ and the regions $\mathcal{W}$, $\mathcal{C}$ and $\mathcal{D}$. Notice that $\mathcal{W}$, $\mathcal{C}$ and $\mathcal{D}$ depend on the position of the true state $\boldsymbol{\rho}_k$, which is unknown. We can decompose the point $\boldsymbol{\rho}_k$ (as well as any measurement $\boldsymbol{z}_k$) in fixed coordinates (ρ_k^x, ρ_k^y) or in wake-oriented coordinates $(\rho_k^{\tilde{x}}, \rho_k^{\tilde{y}})$.

B. Pre-validated measurements

At time k the tracker is fed a set $\tilde{\boldsymbol{Z}}_k = \tilde{\boldsymbol{Z}}_k^1 \cup \tilde{\boldsymbol{Z}}_k^0 \cup \tilde{\boldsymbol{Z}}_k^w$ of measurements from the respective sources of target, background and wake. The tildes indicate that these sets have not yet been subject to validation. In contrast to what was done in Section II, this section takes a parametric viewpoint and assigns informative pmf's to the number of measurements from these sets. In other words, the measurement sets are characterized by their cardinality distributions as well as their distributions of individual member points. The cardinalities are distributed according to

$$\begin{aligned} P\{\mathrm{card}(\tilde{\boldsymbol{Z}}_k^1) = \tau\} =& \mathrm{Bernoulli}(\tau\,;\,P_\mathrm{D}) \\ P\{\mathrm{card}(\tilde{\boldsymbol{Z}}_k^0) = \varphi\} =& \mathrm{Poisson}(\varphi\,;\,\tilde{V}\lambda_0) \\ P\{\mathrm{card}(\tilde{\boldsymbol{Z}}_k^w) = \psi\} =& \mathrm{Poisson}(\psi\,;\,2AB\lambda_w) \end{aligned} \tag{20}$$

where

$$\begin{aligned} \mathrm{Bernoulli}(\tau\,;\,P_\mathrm{D}) &\triangleq \begin{cases} 1-P_\mathrm{D} & \text{if } \tau = 0 \\ P_\mathrm{D} & \text{if } \tau = 1 \\ 0 & \text{otherwise} \end{cases} \\ \mathrm{Poisson}(m\,;\,\lambda) &\triangleq \frac{e^{-\lambda}\lambda^m}{m!}. \end{aligned} \tag{21}$$

The parameters λ_0 and λ_w are the intensities of background and wake, respectively. By $\tilde{V}$ we denote the area of the entire surveillance region. The spatial pdf's of individual measurements are

$$p(\boldsymbol{z}_k|\boldsymbol{z}_k \in \tilde{\boldsymbol{Z}}_k^1, \boldsymbol{x}_k) = \mathcal{N}(\boldsymbol{z}_k\,;\,\boldsymbol{H}\boldsymbol{x}_k, \boldsymbol{R}) \tag{22}$$

$$p(\boldsymbol{z}_k|\boldsymbol{z}_k \in \tilde{\boldsymbol{Z}}_k^0, \boldsymbol{x}_k) = 1/\tilde{V} \tag{23}$$

$$p(\boldsymbol{z}_k|\boldsymbol{z}_k \in \tilde{\boldsymbol{Z}}_k^w, \boldsymbol{x}_k) = \begin{cases} 1/(2AB) & \text{if } \boldsymbol{z} \in \mathcal{W} \\ 0 & \text{otherwise} \end{cases} \tag{24}$$

where $\boldsymbol{z} \in \mathcal{W}$ if and only if $\left\|z^{\tilde{x}}\right\| < A$ and $0 < z^{\tilde{y}} < B$.

C. Post-validated measurements

As mentioned in Section II-B a validation gate is used to prevent the tracking method from wasting resources on measurements very far away from the prediction $\hat{\boldsymbol{z}}_{k|k-1}$. This means that the actual set $\boldsymbol{Z}_k = \boldsymbol{Z}_k^1 \cup \boldsymbol{Z}_k^0 \cup \boldsymbol{Z}_k^w$ encountered by the tracking method is a certain subset of the full set $\tilde{\boldsymbol{Z}}_k$ from Section III-B. The validated measurement sets are given by

$$\boldsymbol{Z}_k^1 = \tilde{\boldsymbol{Z}}_k^1 \cap \mathcal{G},\ \ \boldsymbol{Z}_k^0 = \tilde{\boldsymbol{Z}}_k^0 \cap \mathcal{G},\ \ \boldsymbol{Z}_k^w = \tilde{\boldsymbol{Z}}_k^w \cap \mathcal{C}. \tag{25}$$

The first two of these sets have obvious cardinality pmf's

$$P\{\mathrm{card}(\boldsymbol{Z}_k^1) = \tau \mid \boldsymbol{Z}^{k-1}\} = \mathrm{Bernoulli}(\tau\,;\,P_\mathrm{D}P_\mathrm{G}) \tag{26}$$

$$P\{\mathrm{card}(\boldsymbol{Z}_k^0) = \varphi \mid \boldsymbol{Z}^{k-1}\} = \mathrm{Poisson}(\varphi\,;\,2V_k\lambda_0). \tag{27}$$

The statistics of the validated wake measurement set $\boldsymbol{Z}_k^w$ are less trivial. Difficulties are caused by the fact that the region $\mathcal{C}$ is random, since it depends on the state $\boldsymbol{x}_k$. The cardinality of $\boldsymbol{Z}_k^w$ is no longer Poisson distributed due to the marginalization over $\boldsymbol{x}_k$. Still, a Poisson distribution with parameter $\lambda_w V_k/2$ may serve as an approximation:

$$P\{\mathrm{card}(\boldsymbol{Z}_k^w) = \psi|\boldsymbol{Z}^{k-1}\} \approx \mathrm{Poisson}(\psi\,;\,\lambda_w V_k/2). \tag{28}$$

Since the sum of two Poisson random variables also is Poisson [12 p. 216], the cardinality of general clutter measurements is approximately

$$\begin{aligned} P\{\mathrm{card}(\boldsymbol{Z}_k^w \cup \boldsymbol{Z}_k^0) = \mathrm{n}|\boldsymbol{Z}^{k-1}\} \\ \approx \mathrm{Poisson}(\mathrm{n}\,;\,\lambda_w V_k/2 + \lambda_0 V_k). \end{aligned} \tag{29}$$

The spatial pdf's of a single target or background measurement when conditioned on previous data are

$$\begin{aligned} p(\boldsymbol{z}_k|\boldsymbol{z}_k \in \boldsymbol{Z}_k^1, \boldsymbol{Z}^{k-1}) =& \frac{1}{P_\mathrm{G}}\mathcal{N}(\boldsymbol{z}_k\,;\,\hat{\boldsymbol{z}}_{k|k-1}, \boldsymbol{S}_k) = p_1(i) \\ p(\boldsymbol{z}_k|\boldsymbol{z}_k \in \boldsymbol{Z}_k^0, \boldsymbol{Z}^{k-1}) =& 1/V_k = p_0(i). \end{aligned}$$

Our solution to the wake problem is based on the spatial pdf of validated wake measurements. Since these are to be considered clutter, we focus on the spatial pdf of validated *clutter* measurements $\boldsymbol{z}_k \in \boldsymbol{Z}_k^w \cup \boldsymbol{Z}_k^0$. In Appendix B it is

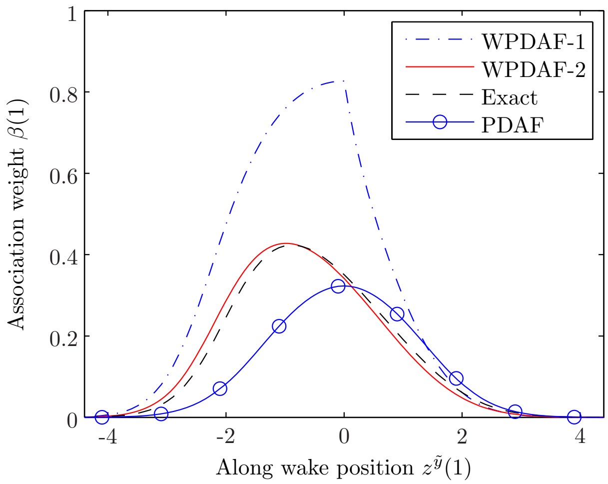

Fig. 2. Comparison of WPDAF-1, WPDAF-2, exact solution and standard PDAF. These curves show the association probability $\beta(1)$ as a function of $\tilde{y}$ for a scenario where $m_k = 2$, $z^{\tilde{x}}(1) = 3$, $z^{\tilde{x}}(2) = 0$, $z^{\tilde{y}}(2) = 5$, $\boldsymbol{P}_{k|k-1} = \boldsymbol{I}$, $\boldsymbol{R} = \boldsymbol{I}$, $g = 6$ and $P_{\mathrm{B}} = \lambda_w/\lambda_0 = 0.9$.

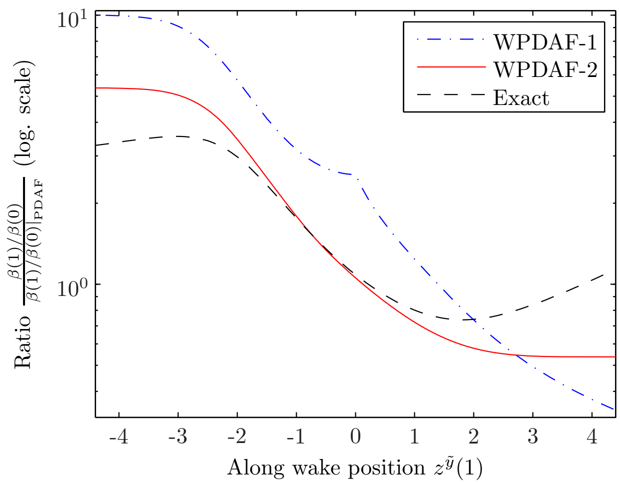

Fig. 3. Comparison of WPDAF-1, WPDAF-2 and exact solution. These curves show how much the association probability of a single measurement is increased or decreased for the WPDAF's relative to the conventional PDAF. The parameters are the same as in Figure 2.

shown that this pdf can be approximated as

$$\begin{aligned} p_w(i) =& p(\boldsymbol{z}_k(i) \,|\, \boldsymbol{z}_k(i) \in \boldsymbol{Z}_k^w \cup \boldsymbol{Z}_k^0, \boldsymbol{Z}^{k-1}) \\ \approx& \frac{1}{\sqrt{\pi^3 |\boldsymbol{\Psi}_k|}} \Bigg[\lambda_0 \left(\frac{2\pi}{2\lambda_0 + \lambda_w} + \frac{32\sqrt{\pi}\lambda_w^2 \alpha^2 \sigma_k^2}{\pi^2 (2\lambda_0 + \lambda_w)^3} \right) \\ &+ \mathrm{ncdf}(z_k^{\tilde{y}}(i)\,;\, 0, \sigma_k^2) \left(\frac{2\sqrt{\pi}\lambda_w}{2\lambda_0 + \lambda_w} + \frac{32\sqrt{\pi}\lambda_w^3 \alpha^2 \sigma_k^2}{\pi^2 (2\lambda_0 + \lambda_w)^3} \right) \\ &+ \exp\left(-\frac{z_k^{\tilde{y}}(i)^2}{2\sigma_k^2} \right) \left(\frac{4\sqrt{2}\lambda_w^2 \alpha \sigma_k}{\pi (2\lambda_0 + \lambda_w)^2} \right. \\ &\quad \left. + \frac{16\sqrt{2}\lambda_w^3 \alpha^2 \sigma_k z_k^{\tilde{y}}(i)}{\pi^2 (2\lambda_0 + \lambda_w)^3} \right) \Bigg] \end{aligned} \tag{30}$$

where

$$\sigma_k^2 = \boldsymbol{u}_k^{\mathsf{T}} \boldsymbol{H} \boldsymbol{P}_{k|k-1} \boldsymbol{H}^{\mathsf{T}} \boldsymbol{u}_k \tag{31}$$

and the scalar α_k is found as

$$\alpha_k = \frac{\|\det(\boldsymbol{B}_k)\|}{\|\boldsymbol{B}_k \cdot [1, 0]^{\mathsf{T}}\|} \tag{32}$$

where $\boldsymbol{B}_k$ is given by an eigenvalue-decomposition

$$\boldsymbol{M}_k \boldsymbol{\Lambda}_k \boldsymbol{M}_k^{\mathsf{T}} = \boldsymbol{\Psi}_k \quad \text{and} \quad \boldsymbol{B}_k = \boldsymbol{\Lambda}_k^{-\frac{1}{2}} \boldsymbol{M}_k^{\mathsf{T}}. \tag{33}$$

By $\mathrm{ncdf}(\cdot)$ we denote the cumulative Gaussian distribution:

$$\mathrm{ncdf}(z\,;\, 0, \sigma^2) = \frac{1}{2} \left(1 + \mathrm{erf}\left(\frac{z}{\sigma\sqrt{2}} \right) \right). \tag{34}$$

Notice that (30) only depends on λ_0 and λ_w through the ratio λ_0/λ_w. It can therefore be used in a non-parametric context as long as one has some idea what this ratio should be.

D. WPDAF-2

The tracking method termed WPDAF-2 is obtained when we replace the mixture (14) with the pdf approximated in (30) of Section III-C:

$$l(i) = \frac{p_1(i)}{p_w(i)}. \tag{35}$$

E. Comparison with exact approach

WPDAF-2 does not provide the exact association probabilities that would result from rigorous Bayesian calculations (cf. Appendix A). The usage of single-measurement likelihood ratios as in (7) and (8) requires the measurements $\boldsymbol{z}_k(1), \ldots, \boldsymbol{z}(m_k)$ to be independent when conditioned on the previous measurements $\boldsymbol{Z}^{k-1}$. The measurements are in general only independent when conditioned on the state $\boldsymbol{x}_k$, and the exact Bayesian solution can therefore only be evaluated numerically by marginalizing the joint density of the entire measurement set $\boldsymbol{Z}_k$ over the predicted density $p(\boldsymbol{x}_k|\boldsymbol{Z}^{k-1})$.

In Figures 2 and 3 the association probabilities of the PDAF, WPDAF-1 and WPDAF-2 as well as the exact approach are illustrated for a scenario with two measurements in the validation gate. It can be seen that WPDAF-1 is in danger of increasing the association probability for measurements that are even significantly behind the prediction. WPDAF-2 does on the other hand exhibit a similar behavior as the exact approach in vicinity of the prediction. Also notice that the ratio between $\beta(i)$ and $\beta(i)|_{\mathrm{PDAF}}$ does not necessarily decrease monotonously as a function of $z^{\tilde{y}}(i)$ for the exact approach. We believe this to be due to the coupling between the measurements in the exact approach.

IV. Test Design and Simulation Results

In this section the trackers known as conventional PDAF, WPDAF-1 and WPDAF-2 (c.f. Sections II-B, II-C and III-D) are tested and compared using Monte-Carlo simulations.

Artificial data can never provide us with the same challenges as real sonar or radar data. However, performance measures such as the occurrence of track-loss can hardly be investigated through real-world experiments. Since (hopefully) track-loss only occurs in a small fraction of all experiments, one must carry out thousands of experiments to obtain statistically valid information. Also, real data will not allow us to investigate the tracking performance as function of model quantities such as the wake strength λ_w.

In [4] the authors tested WPDAF-1 on a single set of real sonar data containing a scuba diver. Its multi-target generalizations have performed well in Monte-Carlo simulations [6, 7]. Still no systematic investigation of its ability to discriminate against wake measurements *alone* has so far been carried out. WPDAF-2 is a novel contribution of this paper, and its performance has consequently never been investigated before.

The methods are here tested on two scenarios which only differ in how artificial wake measurements are generated. In order to test the performance of our tracking methods these scenarios is run 5000 times for 4 different intensities of the wake clutter.

A. Filter model

The tracking methods are implemented using the linear kinematics model given by (1) and (2) with standard matrices given by

$$\boldsymbol{F} = \begin{bmatrix} 1 & T & 0 & 0 \\ 0 & 1 & 0 & 0 \\ 0 & 0 & 1 & T \\ 0 & 0 & 0 & 1 \end{bmatrix}, \ \boldsymbol{Q} = \sigma_v^2 \begin{bmatrix} \frac{T^3}{3} & \frac{T^2}{2} & 0 & 0 \\ \frac{T^2}{2} & T & 0 & 0 \\ 0 & 0 & \frac{T^3}{3} & \frac{T^2}{2} \\ 0 & 0 & \frac{T^2}{2} & T \end{bmatrix}$$

and

$$\boldsymbol{H} = \begin{bmatrix} 1 & 0 & 0 & 0 \\ 0 & 0 & 1 & 0 \end{bmatrix}, \ \boldsymbol{R} = \begin{bmatrix} \sigma_r^2 & 0 \\ 0 & \sigma_r^2 \end{bmatrix}.$$

B. Simulation of target kinematics

As our simulation model we use a more complicated curvilinear model developed in [13]. The curvilinear model is arguably more realistic; modeling colored process noise, manoeuvres and sudden accelerations. In the curvilinear model the state is parameterized as $\boldsymbol{x}_k^{\mathrm{s}} = [x_k, y_k, \dot{x}_k, \dot{y}_k, a_{tk}, a_{nk}]$ where a_{tk} is acceleration tangential to the target trajectory and a_{nk} is acceleration perpendicular to the trajectory. The kinematic process model can then be written as

$$\boldsymbol{x}_{k+1}^{\mathrm{s}} = \begin{bmatrix} \boldsymbol{F} & \boldsymbol{G}_t(\boldsymbol{x}_k^{\mathrm{s}}) & \boldsymbol{G}_n(\boldsymbol{x}_k^{\mathrm{s}}) \\ \boldsymbol{0} & \beta_t & 0 \\ \boldsymbol{0} & 0 & \beta_n \end{bmatrix} \boldsymbol{x}_k^{\mathrm{s}} + \boldsymbol{v}_k^{\mathrm{s}}. \tag{36}$$

The matrices $\boldsymbol{G}_t(\boldsymbol{x}_k^{\mathrm{s}})$ and $\boldsymbol{G}_n(\boldsymbol{x}_k^{\mathrm{s}})$ are explicitly given by

$$\boldsymbol{G}_t(\boldsymbol{x}_k) = \begin{bmatrix} -\frac{1}{\omega_k^2}\cos\varphi_{k+1} + \frac{1}{\omega_k^2}\cos\phi_k - \frac{1}{\omega_k}T\sin\phi_k \\ \frac{1}{\omega_k}\sin\varphi_{k+1} - \frac{1}{\omega_k}\sin\phi_k \\ -\frac{1}{\omega_k^2}\sin\varphi_{k+1} + \frac{1}{\omega_k^2}\sin\phi_k + \frac{1}{\omega_k}T\cos\phi_k \\ -\frac{1}{\omega_k}\cos\varphi_{k+1} + \frac{1}{\omega_k}\cos\phi_k \end{bmatrix}$$

and

$$\boldsymbol{G}_n(\boldsymbol{x}_k) = \begin{bmatrix} -\frac{1}{\omega_k^2}\sin\varphi_{k+1} - \frac{1}{\omega_k^2}\sin\phi_k - \frac{1}{\omega_k}T\cos\phi_k \\ -\frac{1}{\omega_k}\cos\varphi_{k+1} - \frac{1}{\omega_k}\cos\phi_k \\ -\frac{1}{\omega_k^2}\cos\varphi_{k+1} + \frac{1}{\omega_k^2}\cos\phi_k + \frac{1}{\omega_k}T\sin\phi_k \\ \frac{1}{\omega_k}\sin\varphi_{k+1} - \frac{1}{\omega_k}\sin\phi_k \end{bmatrix}$$

where $\varphi_{k+1} = \phi_k + \omega_k T$, $\omega_k = a_{nk}/|\sqrt{\dot{x}_k^2 + \dot{y}_k^2}|$ and $\phi_k = \tan^{-1}(\dot{y}_k/\dot{x}_k)$. The constants β_t and β_n are related to the maneuver time constants τ_t and τ_n by

$$\beta_t = \exp(-T/\tau_t) \ \text{ and } \ \beta_n = \exp(-T/\tau_n).$$

We draw the accelerations according to first order Markov models, so that $\boldsymbol{v}_k^{\mathrm{s}} \sim \mathcal{N}(\boldsymbol{0}, \boldsymbol{Q}^{\mathrm{s}})$ where

$$\boldsymbol{Q}^{\mathrm{s}} = \begin{bmatrix} \boldsymbol{0} & \boldsymbol{0} & \boldsymbol{0} \\ \boldsymbol{0} & \sigma_t^2(1-\beta_t^2) & 0 \\ \boldsymbol{0} & 0 & \sigma_n^2(1-\beta_n^2) \end{bmatrix}. \tag{37}$$

The target moves in a surveillance region covering 500×500m for 300 seconds. The tuning constants σ_t^2, τ_{tm}, σ_n^2 and τ_{nm} have in Table I been chosen such that the kinematics shall mimic a human diver swimming relatively straight ahead.

C. Measurement generation

Measurements are generated according to point processes similar to those described in Section III-B. The simulation of the target and background measurement sets $\boldsymbol{Z}_k^1$ and $\boldsymbol{Z}_k^0$ are straightforward and need no further elaboration. It is less obvious how a realistic wake measurement set $\boldsymbol{Z}_k^w$ should be generated. We will therefore provide two different scenarios. In both scenarios the severity of wake clutter is characterized by a wake intensity ratio r which tells us to which degree the wake clutter dominates over ordinary background clutter.

In Scenario I we draw $\tilde{\boldsymbol{Z}}_k^w$ according to (20) and (24). That is, wake measurements are drawn from a uniform spatial density and the cardinality of $\tilde{\boldsymbol{Z}}_k^w$ is drawn from a Poisson distribution with parameter $2r_sAB\lambda_0$.

In Scenario II we draw $\tilde{\boldsymbol{Z}}_k^w$ according to a recipe similar to the one used in [6]. This recipe draws each wake measurement from a density whose marginal densities are Gaussian and exponentially distributed in the cross-wake and along-wake directions respectively,

$$p(\boldsymbol{z}) = \mathcal{N}(z^{\tilde{x}}\,;\,0, \sigma_s^2) \cdot \frac{1}{\lambda_s}\exp\left(-\frac{z^{\tilde{y}}}{\lambda_s}\right). \tag{38}$$

The cardinality of $\tilde{\boldsymbol{Z}}_k^w$ is drawn from a Poisson distribution with parameter $2r_s\sigma_s\lambda_s\lambda_0$.

The SNR affects the scenario through the detection probability P_{D}. In all our simulations we have used the value $P_{\mathrm{D}} = 0.55$, which corresponds to a 12dB target in Rayleigh noise when the false alarm rate is $P_{\mathrm{FA}} = 0.005$. We assume that the resolution cells of the sensor are $1\mathrm{m} \times 1\mathrm{m}$ wide, implying that the background clutter intensity is $\lambda_0 = 0.005\mathrm{m}^{-2}$. These are values for which PDAF-based trackers are most suitable, and quite realistic in order to model a human diver.

TABLE I

SIMULATION MODEL PARAMETERS

Param.	**Value**	**Specification**
T	$1.0\,\mathrm{s}$	Sampling period
$\Delta_x \times \Delta_y$	$1\mathrm{m} \times 1\mathrm{m}$	Resolution cell size
σ_t^2	$(0.01\,\mathrm{m/s^3})^2$	Tan. acceleration power
τ_{tm}	$2.0\,\mathrm{s}$	Tan. acc. time constant
σ_n^2	$(2.5 \cdot 10^{-5}\,\mathrm{m/s^3})^2$	Perp. acceleration power
τ_{nm}	$1.0\,\mathrm{s}$	Perp. acc. time constant
P_{FA}	0.005	False alarm rate
P_{D}	0.55	Detection probability
$A \times B$	$2.5\mathrm{m} \times 50\mathrm{m}$	Wake region in Scenario I
σ_s	2.5m	Wake half-width in Scenario II
λ_s	10m	Wake length in Scenario II
r_s	$\{1, 5, 10, 50\}$	True wake intensity ratios

TABLE II

FILTER MODEL PARAMETERS

Param.	**Value**	**Specification**
g	6	Gate size
σ_r^2	$(0.0833\,\mathrm{m})^2$	Mea. noise
σ_v^2	$(0.0036\,\mathrm{m/s^2})^2$	Process noise
L	20	Wake direction estimation lag
c_1	3	First stage track-loss threshold
c_2	10	Second stage track-loss threshold
r_a	$\{1, 5, 10, 50\}$	Assumed wake intensity ratios

TABLE III

LOST TRACKS FOR SCENARIO 1

		PDAF	WPDAF-1	WPDAF-2
$r_s = 1$	$r_a = 1$	5	8	1
	$r_a = 5$	5	61	16
	$r_a = 10$	5	152	46
	$r_a = 50$	5	655	190
$r_s = 5$	$r_a = 1$	62	20	10
	$r_a = 5$	62	56	9
	$r_a = 10$	62	141	31
	$r_a = 50$	62	634	184
$r_s = 10$	$r_a = 1$	325	50	46
	$r_a = 5$	325	64	23
	$r_a = 10$	325	139	32
	$r_a = 50$	325	606	172
$r_s = 50$	$r_a = 1$	4993	183	336
	$r_a = 5$	4993	109	84
	$r_a = 10$	4993	132	84
	$r_a = 50$	4993	405	109

TABLE IV

LOST TRACKS FOR SCENARIO 2

		PDAF	WPDAF-1	WPDAF-2
$r_s = 1$	$r_a = 1$	43	17	11
	$r_a = 5$	43	51	12
	$r_a = 10$	43	106	24
	$r_a = 50$	43	532	141
$r_s = 5$	$r_a = 1$	659	105	76
	$r_a = 5$	659	67	37
	$r_a = 10$	659	99	46
	$r_a = 50$	659	374	93
$r_s = 10$	$r_a = 1$	749	82	48
	$r_a = 5$	749	77	51
	$r_a = 10$	749	99	59
	$r_a = 50$	749	273	87
$r_s = 50$	$r_a = 1$	543	53	29
	$r_a = 5$	543	75	57
	$r_a = 10$	543	88	66
	$r_a = 50$	543	125	71

D. Performance measures

In the same way as was done in [2], this paper uses track-loss as the primary performance measure. We treat track-loss as a two-stage process. A track is considered tentatively lost at time k if the position error $\sqrt{(x_{k|k} - x_k^{\mathrm{s}})^2 + (y_{k|k} - y_k^{\mathrm{s}})^2}$ exceeds a threshold c_1. If the error later goes below c_1 the lost label is removed. On the other hand, if the error never manages to go below c_1 again, we consider it lost at time k. If the error exceeds the higher threshold $c_2 > c_1$ we immediately consider it lost at time k, irrespectively on whether the error later goes below c_1.

E. Interpretation of the results

Tables III and IV provide a summary of our results. We point out the following observations:

First, it can be seen that the strength of wake clutter is critical to the performance of the PDAF. The PDAF does cope reasonably well with moderate wake intensities in Scenario I, although a quite significant performance loss is apparent. For very high wake intensities ($\lambda_w \geq 50\lambda_0$) the PDAF looses track inevitably. In Scenario II moderate wake intensities are most troublesome, while stronger wakes are easier to handle, probably because the exponential distribution places a large number of wake measurements close to the target.

Second, it can be seen that both WPDAF-1 and WPDAF-2 may reduce the track-loss encountered by the PDAF. Their mitigating effect is as one would expect most prominent for strong wakes. WPDAF-2 does in the vast majority of cases outperform WPDAF-1, and especially so when the true wake intensity is weak. Unfortunately, neither WPDAF-1 nor WPDAF-2 can be guaranteed to improve performance. There is a danger that the tracker will push the state estimate too far ahead when it assumes the wake to be stronger than it actually is. This may cause it to loose track. We see this happening more frequently for WPDAF-1 than for WPDAF-2.

Third, the WPDAF's do not necessarily achieve their best performance for the correct wake intensity ratio $r_a = r_s$. Although WPDAF-1 was run with rather high values of r_a in [6] and [4], the results presented in Tables III and IV indicate that lower values of r_a should be used for WPDAF-1. The novel tracker WPDAF-2 does on the other hand most often attain its optimal performance when r_a is equal to or reasonably near r_s. It is nevertheless also for WPDAF-2 safer to assume a too low wake intensity than a too high wake intensity.

V. Conclusion

This paper has studied the performance of three PDAF-based methods for tracking targets with wakes. These are the conventional PDAF, a recently developed modification based on probabilistic editing (WPDAF-1), and a tracker developed in this paper by means of marginalization (WPDAF-2). Simulation results have revealed that a significant performance gain can be achieved by accounting for the wake as done in WPDAF-1 and WPDAF-2, and that this gain is most prominent and consistent for WPDAF-2.

There are at least two alleys for further research that this paper leads to. Since both WPDAF-1 and WPDAF-2 do exhibit some sensitivity to the assumed wake strength, it is of great interest to develop robust estimators for this quantity. WPDAF-1 is purely non-parametric, and it is difficult to see how estimation of the wake strength can be done for it. WPDAF-2 is on the other hand developed in a parametric framework, so that such an estimation does make more sense for this tracker. Exactly what kind of estimators would be preferable is not that obvious. The approaches of [14] or [15] may provide some inspiration for this.

This paper has solely focused on track maintenance, i.e. whether or not the tracker manages to follow the target. Another important topic for future research is track initialization and termination in the presence of wake clutter. While simple heuristic rules were used successfully in [4] and [7], it would be interesting to replace these with a more systematic approach such as the Integrated Probabilistic Data Association (IPDA) [16] or random set methods [8].

Appendix

Non-trivial calculations underlying the results of this paper are placed in three appendices. The first appendix explains how the PDAF can be written by means of likelihood ratios. The second appendix derives the spatial clutter pdf of WPDAF-2, which is the main result of this paper.

A. The role of likelihood ratios in the PDAF

The PDAF is derived under the assumption of a uniform spatial clutter pdf [5 pp. 129-161]. This assumption conveniently allows us to express the association probabilities (7) and (8) using likelihood ratios $l(i)$ of the individual measurements conditioned on previous data. When the spatial clutter pdf depends on $\boldsymbol{x}_k$ this de-coupling breaks down. Approximations, whose nature is the topic of this appendix, are then necessary to maintain this simplicity.

Let m_k and n_k be the number of total and clutter measurements respectively at time k, and let m be the realization of the random variable m_k. Bayes' rule yields

$$\begin{aligned} P\{\theta_k(0)|\boldsymbol{Z}^k\} =& P\{\theta_k(0)|m_k, \boldsymbol{Z}_k, \boldsymbol{Z}^{k-1}\} \\ =& \frac{1}{c} p(\boldsymbol{Z}_k|\theta_k(0), m_k, \boldsymbol{Z}^{k-1}) \\ & \cdot P\{\theta_0|n_k = \mathrm{m}, m_k = \mathrm{m}\} \\ & \cdot P\{n_k = \mathrm{m}|m_k = \mathrm{m}\} \end{aligned} \tag{39}$$

and

$$\begin{aligned} P\{\theta_k(i)|\boldsymbol{Z}^k\} =& P\{\theta_k(i)|m_k, \boldsymbol{Z}_k, \boldsymbol{Z}^{k-1}\} \\ =& \frac{1}{c} p(\boldsymbol{Z}_k|\theta_k(i), m_k, \boldsymbol{Z}^{k-1}) \\ & \cdot P\{\theta_i|n_k = \mathrm{m}-1, m_k = \mathrm{m}\} \\ & \cdot P\{n_k = \mathrm{m}-1|m_k = \mathrm{m}\}. \end{aligned} \tag{40}$$

The joint measurement pdf's $p(\boldsymbol{Z}_k|\theta_k(0), m_k, \boldsymbol{Z}^{k-1})$ and $p(\boldsymbol{Z}_k|\theta_k(i), m_k, \boldsymbol{Z}^{k-1})$ are conditioned on the past data (as represented by the prediction and its covariance) and not on the state $\boldsymbol{x}_k$. However, since target and clutter measurements depend on the state rather than the prediction, these quantities must be written as integrals over the state,

$$\begin{aligned} p(\boldsymbol{Z}_k|\theta_k(0), \ldots) &= \int \prod_{j=1}^{m_k} p_c(\boldsymbol{z}_k(j)|\boldsymbol{x}_k) p(\boldsymbol{x}_k|\boldsymbol{Z}^{k-1}) \mathrm{d}\boldsymbol{x}_k \\ p(\boldsymbol{Z}_k|\theta_k(i), \ldots) &= \int p_1(\boldsymbol{z}_k(i)|\boldsymbol{x}_k) \prod_{j\neq i}^{m_k} p_c(\boldsymbol{z}_k(j)|\boldsymbol{x}_k) \\ & \qquad \cdot p(\boldsymbol{x}_k|\boldsymbol{Z}^{k-1}) \mathrm{d}\boldsymbol{x}_k. \end{aligned} \tag{41}$$

Here $p_1(\cdot|\boldsymbol{x}_k)$ is the spatial pdf of target measurements and $p_c(\cdot|\boldsymbol{x}_k)$ is the spatial pdf of clutter measurements conditioned on the state.

In the conventional PDAF only $p_1(\cdot|\boldsymbol{x}_k)$ depends on the state, while $p_c(\cdot|\boldsymbol{x}_k) = p_c(\cdot)$ is uniform. The integrals in (41) are then of a trivial nature. However, in the treatment of wake clutter we allow $p_c(\cdot|\boldsymbol{x}_k)$ to depend on the state, which results in non-trivial marginalization integrals. An "exact" Bayesian approach along the lines of [9] would solve these integrals numerically (c.f. Section III-E). A simpler, although somewhat heuristic, approach is to approximate the integrals by assuming that the the measurements $\boldsymbol{z}_k(1), \ldots, \boldsymbol{z}_k(m_k)$ are independent, not only when conditioned on the state $\boldsymbol{x}_k$, but also when conditioned on the previous data $\boldsymbol{Z}^{k-1}$. We simply proceed as if the joint measurement pdf's also in this case can be decoupled as follows:

$$p(\boldsymbol{Z}_k|\theta_k(0),\ldots) \approx \prod_{j=1}^{m_k} \int p_c(\boldsymbol{z}_k(j)|\boldsymbol{x}_k)p(\boldsymbol{x}_k|\boldsymbol{Z}^{k-1})\mathrm{d}\boldsymbol{x}_k = \prod_{j=1}^{m_k} p_c(j) \tag{42}$$

$$p(\boldsymbol{Z}_k|\theta_k(i),\ldots) \approx \int p_1(\boldsymbol{z}_k(i)|\boldsymbol{x}_k)p(\boldsymbol{x}_k|\boldsymbol{Z}^{k-1})\mathrm{d}\boldsymbol{x}_k \cdot \prod_{j\neq i}^{m_k} \int p_c(\boldsymbol{z}_k(j)|\boldsymbol{x}_k)p(\boldsymbol{x}_k|\boldsymbol{Z}^{k-1})\mathrm{d}\boldsymbol{x}_k = p_1(i)\prod_{j\neq i}^{m_k} p_c(j) = l(i)\prod_{j=1}^{m_k} p_c(j). \tag{43}$$

The inverse association probabilities can then be found as

$$\frac{1}{P\{\theta_k(0)|\boldsymbol{Z}^k\}} = \frac{\chi}{\mathrm{m}\prod_{j=1}^{\mathrm{m}} p_c(j)(1-P_\mathrm{D}P_\mathrm{G})\mu(\mathrm{m})} = 1 + \frac{P_\mathrm{D}P_\mathrm{G}}{\mathrm{m}(1-P_\mathrm{D}P_\mathrm{G})}\frac{\mu(\mathrm{m}-1)}{\mu(\mathrm{m})}\sum l(j)$$

and

$$\frac{1}{P\{\theta_k(i)|\boldsymbol{Z}^k\}} = \frac{\chi}{l(i)\prod_{j=1}^{\mathrm{m}} p_c(j)P_\mathrm{D}P_\mathrm{G}\mu(\mathrm{m}-1)} = \frac{1}{l(i)}\left(\frac{\mathrm{m}(1-P_\mathrm{D}P_\mathrm{G})}{P_\mathrm{D}P_\mathrm{G}}\frac{\mu(\mathrm{m})}{\mu(\mathrm{m}-1)} + \sum l(j)\right)$$

where another normalization constant has been introduced as

$$\chi = \mathrm{m}\prod_{j=1}^{\mathrm{m}} p_c(j)(1-P_\mathrm{D}P_\mathrm{G})\mu(\mathrm{m}) + P_\mathrm{D}P_\mathrm{G}\mu(\mathrm{m}-1)\prod_{j=1}^{m_k} p_c(j)\sum_{j=1}^{m_k} l(j).$$

For the case of a non-parametric PDAF the ratio $\mu(\mathrm{m})/\mu(\mathrm{m}-1)$ is by definition unity. Under that assumption the association probabilities in (7) and (8) follow immediately.

B. Single point clutter likelihood in WPDAF-2

In this appendix we derive the approximation (30) of the spatial pdf for elements of $\boldsymbol{Z}_k^0 \cup \boldsymbol{Z}_k^w$. This treatment will take place in the wake oriented coordinate system $(\tilde{x}, \tilde{y})$ under the following three assumptions

- A1: The validation gate $\mathcal{G}$ is so large that $P_\mathrm{G} \approx 1$.
- A2: The rectangular wake region $\mathcal{W}$ is so large that none of its corners can fall inside $\mathcal{G}$ as long as $\boldsymbol{x}_k \in \mathcal{G}$.
- A3: The event $\theta_k(i)$ is not true, i.e. $\boldsymbol{z}_k(i) \in \boldsymbol{Z}_k^w \cup \boldsymbol{Z}_k^0$.

Clearly these assumptions cannot be guaranteed to hold. Situations where A1 and A2 cannot both hold, will in reality occur quite frequently. Such violations do not primarily have an impact on the qualitative properties of the spatial clutter pdf, rather they mean that the actual number of wake measurements may differ significantly from the expected number of wake measurements. For parametric tracking methods which attempt to draw inference from the number of measurements this could have dangerous consequences, but it should not pose a serious problem in the non-parametric setting.

By the total probability theorem we have

$$\begin{aligned} &p(\boldsymbol{z}_k|\boldsymbol{z}_k \in \boldsymbol{Z}_k^w \cup \boldsymbol{Z}_k^0,\, \boldsymbol{Z}^{k-1}) \\ &= \int p(\boldsymbol{z}_k|\boldsymbol{x}_k, \boldsymbol{Z}^{k-1})p(\boldsymbol{x}_k|\boldsymbol{Z}^{k-1})\mathrm{d}\boldsymbol{x}_k \\ &= \int [p(\boldsymbol{z}_k|\boldsymbol{z}_k \in \mathcal{C})P\{\boldsymbol{z}_k \in \mathcal{C}|\boldsymbol{x}_k\} \\ &\quad + p(\boldsymbol{z}_k|\boldsymbol{z}_k \in \mathcal{D})P\{\boldsymbol{z}_k \in \mathcal{D}|\boldsymbol{x}_k\}]\, p(\boldsymbol{x}_k|\boldsymbol{Z}^{k-1})\mathrm{d}\boldsymbol{x}_k. \end{aligned} \tag{44}$$

Since the state conditioned clutter likelihoods are uniform inside their (unknown) support regions we will work with expressions for the areas of $\mathcal{C}$ and $\mathcal{D}$. Due to assumption A2 the value of $\rho_k^{\tilde{x}}$ is irrelevant and it suffices to express these areas as functions of $\rho_k^{\tilde{y}}$. If the areas of $\mathcal{C}(\boldsymbol{\rho}_k)$ and $\mathcal{D}(\boldsymbol{\rho}_k)$ are denoted by $C(\rho_k^{\tilde{y}})$ and $D(\rho_k^{\tilde{y}})$ respectively, we can write

$$C(\rho_k^{\tilde{y}}) = \begin{cases} C_1(\rho_k^{\tilde{y}}) & \text{if } \rho_k^{\tilde{y}} <= 0 \\ C_2(\rho_k^{\tilde{y}}) & \text{if } \rho_k^{\tilde{y}} > 0 \end{cases}$$

$$D(\rho_k^{\tilde{y}}) = \begin{cases} D_1(\rho_k^{\tilde{y}}) & \text{if } \rho_k^{\tilde{y}} <= 0 \\ D_2(\rho_k^{\tilde{y}}) & \text{if } \rho_k^{\tilde{y}} > 0 \end{cases}$$

where

$$C_1(\rho_k^{\tilde{y}}) = \Xi_k\left[\pi - \operatorname{acos}(-\alpha\rho_k^{\tilde{y}}) + \frac{1}{2}\sin\left(2\operatorname{acos}(-\alpha\rho_k^{\tilde{y}})\right)\right]$$

$$D_1(\rho_k^{\tilde{y}}) = \Xi_k\left[\operatorname{acos}(-\alpha\rho_k^{\tilde{y}}) - \frac{1}{2}\sin\left(2\operatorname{acos}(-\alpha\rho_k^{\tilde{y}})\right)\right]$$

$$C_2(\rho_k^{\tilde{y}}) = \Xi_k\left[\operatorname{acos}(\alpha\rho_k^{\tilde{y}}) - \frac{1}{2}\sin\left(2\operatorname{acos}(\alpha\rho_k^{\tilde{y}})\right)\right]$$

$$D_2(\rho_k^{\tilde{y}}) = \Xi_k\left[\pi - \operatorname{acos}(\alpha\rho_k^{\tilde{y}}) + \frac{1}{2}\sin\left(2\operatorname{acos}(\alpha\rho_k^{\tilde{y}})\right)\right]$$

with α given by (32) and $\Xi_k = \sqrt{|\boldsymbol{\Psi_k}|}$. The probabilities that a single clutter measurement $\boldsymbol{z}_k$ is in $\mathcal{C}$ or $\mathcal{D}$ can be found as

$$P\{\boldsymbol{z}_k \in \mathcal{C}|\boldsymbol{x}_k\} = \frac{(\lambda_0+\lambda_w)C(\rho_k^{\tilde{y}})}{(\lambda_0+\lambda_w)C(\rho_k^{\tilde{y}}) + \lambda_0 D(\rho_k^{\tilde{y}})}$$

$$P\{\boldsymbol{z}_k \in \mathcal{D}|\boldsymbol{x}_k\} = \frac{\lambda_0 D(\rho_k^{\tilde{y}})}{(\lambda_0+\lambda_w)C(\rho_k^{\tilde{y}}) + \lambda_0 D(\rho_k^{\tilde{y}})}.$$

Therefore, the spatial clutter likelihood conditioned on $\boldsymbol{x}_k$ is

$$p(\boldsymbol{z}_k|\boldsymbol{x}_k) = \begin{cases} \frac{(\lambda_0+\lambda_w)}{(\lambda_0+\lambda_w)C(\rho_k^{\tilde{y}})+\lambda_0 D(\rho_k^{\tilde{y}})} & \text{if } \boldsymbol{z}_k \in \mathcal{C}(\boldsymbol{x}_k) \\ \frac{\lambda_0}{(\lambda_0+\lambda_w)C(\rho_k^{\tilde{y}})+\lambda_0 D(\rho_k^{\tilde{y}})} & \text{if } \boldsymbol{z}_k \in \mathcal{D}(\boldsymbol{x}_k). \end{cases}$$

We can then rewrite (44) as

$$\begin{aligned} &p(\boldsymbol{z}_k|\boldsymbol{z}_k \in \boldsymbol{Z}_k^w \cup \boldsymbol{Z}_k^0,\, \boldsymbol{Z}^{k-1}) \\ &= (\lambda_0+\lambda_w)\int_{\mathcal{G}^*} \frac{\mathcal{N}(\boldsymbol{x}_k\,;\,\hat{\boldsymbol{x}}_{k|k-1}, \boldsymbol{P}_{k|k-1})}{(\lambda_0+\lambda_w)C(\rho_k^{\tilde{y}}) + \lambda_0 D(\rho_k^{\tilde{y}})}\chi_{\mathcal{C}(\boldsymbol{x}_k)}(\boldsymbol{z}_k)\mathrm{d}\boldsymbol{x}_k \\ &\quad + \lambda_0\int_{\mathcal{G}^*} \frac{\mathcal{N}(\boldsymbol{x}_k\,;\,\hat{\boldsymbol{x}}_{k|k-1}, \boldsymbol{P}_{k|k-1})}{(\lambda_0+\lambda_w)C(\rho_k^{\tilde{y}}) + \lambda_0 D(\rho_k^{\tilde{y}})}\chi_{\mathcal{D}(\boldsymbol{x}_k)}(\boldsymbol{z}_k)\mathrm{d}\boldsymbol{x}_k \end{aligned} \tag{45}$$

where $\mathcal{G}^* \triangleq \mathcal{G} \times \mathbb{R}^2$ and $\chi_\mathcal{C}(\cdot)$ and $\chi_\mathcal{D}(\cdot)$ denote the characteristic functions [17 p. 46] of the regions $\mathcal{C}$ and $\mathcal{D}$.

Some manipulations of these and integration over all variables in $\boldsymbol{x}_k$ but $\rho_k^{\tilde{y}}$ yields

$$
\begin{aligned}
&p(\boldsymbol{z}_k|\boldsymbol{z}_k \in \boldsymbol{Z}_k^w \cup \boldsymbol{Z}_k^0,\, \boldsymbol{Z}^{k-1}) \qquad (46)\\
=&\frac{\lambda_0+\lambda_w}{\sigma\sqrt{2\pi}}\int_{-\infty}^{z_k^{\tilde{y}}}\frac{\exp\left(-(\rho_k^{\tilde{y}})^2/2\sigma^2\right)}{(\lambda_0+\lambda_w)C(\rho_k^{\tilde{y}})+\lambda_0 D(\rho_k^{\tilde{y}})}\mathrm{d}\rho_k^{\tilde{y}}\\
&+\frac{\lambda_0}{\sigma\sqrt{2\pi}}\int_{z_k^{\tilde{y}}}^{\infty}\frac{\exp\left(-(\rho_k^{\tilde{y}})^2/2\sigma^2\right)}{(\lambda_0+\lambda_w)C(\rho_k^{\tilde{y}})+\lambda_0 D(\rho_k^{\tilde{y}})}\mathrm{d}\rho_k^{\tilde{y}}.
\end{aligned}
$$

The challenge posed by the function

$$
g_l(\rho_k^{\tilde{y}}) = \frac{1}{(\lambda_0+\lambda_w)C_l(\rho_k^{\tilde{y}})+\lambda_0 D_l(\rho_k^{\tilde{y}})},\; l\in\{1,2\}
$$

can only be overcome by some kind of approximation. In order to obtain a closed form approximation to (44), a series expansion approach can be used. Since the Gaussian has the bulk of its probability mass close to zero in wake oriented $(\tilde{x},\tilde{y})$-coordinates, we expand $g_1(\rho_k^{\tilde{y}})$ around $\rho_k^{\tilde{y}} = 0$ up to second order. This requires the first and second order derivatives of $C_1(\rho_k^{\tilde{y}})$ and $D_1(\rho_k^{\tilde{y}})$. The details are messy, so we only summarize the results here:

$$
\begin{aligned}
g_1(0) &= \frac{2}{\pi\sqrt{|\Psi|}(2\lambda_0+\lambda_w)}\\
g_1'(0) &= \frac{8\lambda_w\alpha}{\pi^2\sqrt{|\Psi|}(2\lambda_0+\lambda_w)^2}\\
g_1''(0) &= \frac{64\lambda_w^2\alpha^2}{\pi^3\sqrt{|\Psi|}(2\lambda_0+\lambda_w)^3}. \qquad (47)
\end{aligned}
$$

We can then approximate $g_l(\rho_k^{\tilde{y}})$ with the function

$$
\begin{aligned}
g(\rho_k^{\tilde{y}}) =&\frac{2}{\pi\sqrt{|\Psi|}(2\lambda_0+\lambda_w)}+\rho_k^{\tilde{y}}\frac{8\lambda_w\alpha}{\pi^2\sqrt{|\Psi|}(2\lambda_0+\lambda_w)^2}\\
&+(\rho_k^{\tilde{y}})^2\frac{32\lambda_w^2\alpha^2}{\pi^3\sqrt{|\Psi|}(2\lambda_0+\lambda_w)^3}. \qquad (48)
\end{aligned}
$$

Inserting (48) into (46) yields 6 terms on the form $\int(\rho_k^{\tilde{y}})^n\exp(-(\rho_k^{\tilde{y}})^2/2\sigma^2)\mathrm{d}\rho_k^{\tilde{y}}$, which all can be integrated in closed form [18 pp. 108-109]. Evaluation of these integrals yields (30). The adequacy of this approximation is illustrated in Figure 4.

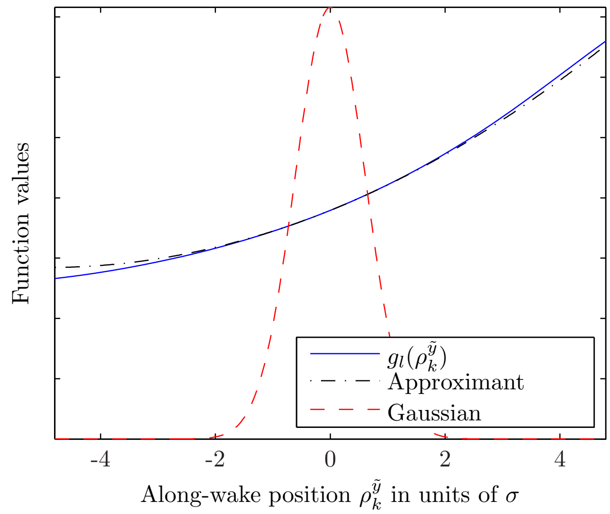

Fig. 4. Adequacy of the approximation (48). It can be seen that the 2nd order approximation $g(\rho_k^{\tilde{y}})$ is as good as identical with $g_l(\rho_k^{\tilde{y}})$ over the effective support of the Gaussian $\mathcal{N}(\rho_k^{\tilde{y}}\,; 0, \sigma^2)$.

References

[1] P. P. Gandhi and S. A. Kassam, "Analysis of CFAR Processors in Non-Homogeneous Background," *IEEE Transactions on Aerospace and Electronic Systems*, vol. 24, no. 4, pp. 427–445, Jul. 1988.

[2] E. Brekke, O. Hallingstad, and J. Glattetre, "Tracking Small Targets in Heavy-Tailed Clutter Using Amplitude Information," accepted for publication in IEEE Journal of Oceanic Engineering.

[3] M. Athans, R. Whiting, and M. Gruber, "A Suboptimal Estimation Algorithm with Probabilistic Editing for False Measurements with Applications to Target Tracking with Wake Phenomena," *IEEE Transactions on Automatic Control*, vol. 22, no. 3, pp. 372–384, Jun. 1977.

[4] A. Rødningsby and Y. Bar-Shalom, "Tracking of Divers using a Probabilistic Data Association Filter with a Bubble Model," *IEEE Transactions on Aerospace and Electronic Systems*, vol. 45, no. 3, pp. 1181–1193, Jul. 2009.

[5] Y. Bar-Shalom and X. R. Li, *Multitarget-Multisensor Tracking: Principles and Techniques*. Storrs, CT, USA: YBS Publishing, 1995.

[6] A. Rødningsby, Y. Bar-Shalom, O. Hallingstad, and J. Glattetre, "Multitarget Tracking in the Presence of Wakes," in *Proceedings of the 11th International Conference on Information Fusion*, Cologne, Jun./Jul. 2008, pp. 1–8.

[7] ——, "Multitarget Multisensor Tracking in the Presence of Wakes," accepted for publication in Journal of Advances in Information Fusion.

[8] R. Mahler, *Statistical Multisource-Multitarget Information Fusion*. Artech House, 2007.

[9] B.-T. Vo, B.-N. Vo, and A. Cantoni, "Bayesian Filtering With Random Finite Set Observations," *IEEE Transactions on Signal Processing*, vol. 56, no. 4, pp. 1313–1326, Apr. 2008.

[10] A. Gelb, *Applied Optimal Estimation*. MIT Press, 1973.

[11] E. Brekke, O. Hallingstad, and J. Glattetre, "Improved Target Tracking in the Presence of Wakes," 2010, submitted to IEEE Transactions on Aerospace and Electronic Systems.

[12] A. Papoulis and S. U. Pillai, *Probability, Random Variables and Stochastic Processes*. McGraw-Hill, 2002.

[13] R. A. Best and J. P. Norton, "A New Model And Efficient Tracker For A Target With Curvilinear Motion," *IEEE Transactions on Aerospace and Electronic Systems*, vol. 33, no. 3, pp. 1030–1037, Jul. 1997.

[14] X. R. Li and N. Li, "Integrated Real-Time Estimation of Clutter Density for Tracking," *IEEE Transactions on Signal Processing*, vol. 48, no. 10, pp. 2797–2805, Oct. 2000.

[15] D. Musicki, S. Suvorova, M. Morelande, and B. Moran, "Clutter Map and Target Tracking," in *Proceedings of the 8th International Conference on Information Fusion*, Philadelphia, PA, USA, Jul. 2005.

[16] D. Musicki, R. Evans, and S. Stankovic, "Integrated Probabilistic Data Association," *IEEE Transactions on Automatic Control*, vol. 39, no. 6, pp. 1237–1241, 1994.

[17] G. B. Folland, *Real Analysis: Modern Techniques and Their Applications*. Wiley, 1999.

[18] I. Gradshteyn and I. Ryzhik, *Table of Integrals, Series, and Products*, 7th ed., D. Zwillinger, Ed. Academic Press, Elsevier Inc., 2007.